Contribution from the Department of Chemistry,
University of Geneva, 1211 Geneva 4, Switzerland

Electronic Structure and Spectroscopic Properties of Chromium(V), Molybdenum(VI), and Niobium(V) Tetraperoxides

M. ROCH, J. WEBER,* and A. F. WILLIAMS

Received March 7, 1984

SCF–MS–Xα molecular orbital calculations are reported for the ions $[Cr(O_2)_4]^{3-}$, $[Mo(O_2)_4]^{2-}$, and $[Nb(O_2)_4]^{3-}$. The bonding is discussed in terms of the interaction between the metal ion and four peroxide fragments: the strongest interaction is that between the metal orbitals and the peroxide π_g^* orbital in the plane of the MO_2 fragment, but the π_u bonding orbitals also act as donors to the metal. The electronic structure of the Mo(VI) complex is markedly different from that of the other members of the series: the peroxide σ_g(p) orbitals are significantly involved in the covalent interactions with molybdenum 4d orbitals, which results in a strong disruption of the σ_g(p) levels. In addition, it is in this complex that the O–O bond is most weakened and the dioxygen ligands acquire some electrophilic character, which is undoubtedly to be related with the unique catalytic properties of Mo(VI) dioxygen complexes for the epoxidation of alkenes. The calculated optical and EPR spectra of the complexes are in good agreement with experimental data. Finally, the SCF–MS–Xα wave functions have been used to calculate the electron deformation density in the $[Cr(O_2)_4]^{3-}$ ion.

Introduction

Mononuclear transition-metal complexes containing dioxygen ligands[1] have recently been the subject of numerous experimental[2,3] and theoretical[1,4] studies. In addition to addressing the problem of the nature of the chemical bond between dioxygen and metal atom in compounds such as hemoglobin and hemoproteins, these investigations aim at understanding the well-known catalytic behavior of these complexes in some important chemical reactions.[5-7] Most of the studies that have appeared so far have attempted to make correlations between the mode of dioxygen coordination and the chemical properties of these complexes. As such, they are generally based on crude or qualitative models of predicting the electronic structure of metal dioxygen units, and with the exception of oxyhemoglobin, relatively few high-quality calculations on metal dioxygen complexes have been published.[8-12]

In this paper, we present the results of a detailed molecular orbital (MO) study of the peroxo complexes $[Cr(O_2)_4]^{3-}$, $[Mo(O_2)_4]^{2-}$, and $[Nb(O_2)_4]^{3-}$, performed by using the SCF–MS–Xα model, which has recently been shown to give quantitatively reliable predictions of the electronic structure and related properties of coordination and organometallic compounds.[13-15] These $[MO_8]^{n-}$ anions are among the simplest compounds exhibiting metal–dioxygen bonds, and they contain four sideways-coordinated (η^2) dioxygen units (I).

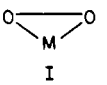

I

The high symmetry of the $[MO_8]^{n-}$ complexes (D_{2d}, corresponding roughly to a tetrahedral disposition of the sideways-bonded O_2 groups about the metal atom) makes them attractive subjects for calculations and also simplifies the interpretation of spectroscopic data. In this investigation, we are interested in the following points: (i) the nature of the metal–dioxygen bond in the $M(O_2)$ unit; (ii) its relationship to the catalytic properties of some Mo peroxide compounds; (iii) the interpretation of the optical and UV absorption spectra of the compounds; (iv) the calculation of both the electron deformation density distribution and hyperfine tensor on the metal in $[Cr(O_2)_4]^{3-}$.

Table I. Calculation Parameters

	$[Cr(O_2)_4]^{3-}$	$[Mo(O_2)_4]^{2-}$	$[Nb(O_2)_4]^{3-}$
	α Values		
metal	0.713 52	0.703 41	0.703 83
oxygen	0.744 47	0.744 47	0.744 47
outer sphere + inter sphere	0.741 03	0.739 91	0.739 95
	Sphere Radii,[a] au		
metal	2.178 23	2.332 53	2.423 70
oxygen 1	1.819 70	1.851 33	1.831 97
oxygen 2	1.807 23	1.831 80	1.825 01
outer sphere	5.519 84	5.630 84	5.692 68

[a] Oxygen atoms 1 and 2 are depicted in Figure 1.

Calculations

The standard version of the SCF–MS–Xα method[16] was used. This model has been described in detail several times[16-18] and needs no further discussion here. However, some computational details, as well as the choice of the calculation parameters, deserve some comment since they have been shown to have a tangible influence on the results.

Each complex was assumed to have D_{2d} symmetry (Figure 1), the geometries being taken from recent crystallographic studies:[8,19,20]

(1) Gubelmann, M. H.; Williams, A. F. *Struct. Bonding (Berlin)* **1983**, *55*, 1.
(2) Vaska, L. *Acc. Chem. Res.* **1976**, *9*, 175.
(3) Lever, A. B. P.; Gray, H. B. *Acc. Chem. Res.* **1978**, *11*, 348.
(4) Summerville, D. A.; Jones, R. D.; Hoffman, B. M.; Basolo, F. *J. Chem. Educ.* **1979**, *56*, 157.
(5) (a) The First International Symposium on Activation of Molecular Oxygen and Selective Oxidation Catalyzed by Transition Metal Complexes; Bendor: France; 1979. *J. Mol. Catal.* **1980**, *7*, 1. (b) Lyons, J. E. "Fundamental Research in Homogeneous Catalysis"; Tsutsui, M., Ugo, R., Eds.; Plenum Press: New York, 1977; pp 1–52.
(6) Collman, J. P.; Chang, A. O.; Jameson, G. B.; Oakley, R. T.; Rose, E.; Schmitton, E. R.; Ibers, J. A. *J. Am. Chem. Soc.* **1981**, *103*, 516.
(7) (a) *Spec. Publ.—Chem. Soc.* **1981**, *No. 39*. (b) Spiro, T. G., Ed.; "Metal Ion Activation of Dioxygen"; Wiley: New York, 1980. (c) Caughey, W. S., Ed.; "Biochemical and Clinical Aspects of Oxygen"; Academic Press: New York, 1979.
(8) Fischer, J.; Veillard, A.; Weiss, R. *Theor. Chim. Acta* **1972**, *24*, 317.
(9) Dedieu, A.; Rohmer, M. M.; Veillard, H.; Veillard, A. *Nouv. J. Chim.* **1979**, *3*, 653 and references cited therein.
(10) Dacre, P. D.; Elder, M. *J. Chem. Soc., Dalton Trans.* **1972**, 1426.
(11) Case, D. A.; Huynh, B. H.; Karplus, M. *J. Am. Chem. Soc.* **1979**, *101*, 4433.
(12) Norman, J. G.; Ryan, P. B. *Inorg. Chem.* **1982**, *21*, 3555.
(13) Weber, J.; Goursot, A.; Pénigault, E.; Ammeter, J. H.; Bachmann, J. *J. Am. Chem. Soc.* **1982**, *104*, 1451.
(14) Weber, J. In "Current Aspects of Quantum Chemistry 1981"; Carbo, R., Ed.; Elsevier: Amsterdam, 1982; pp 437–450.
(15) Case, D. A. *Ann. Rev. Phys. Chem.* **1982**, *33*, 151.
(16) Johnson, K. H. *Adv. Quantum Chem.* **1973**, *7*, 143.
(17) Slater, J. C. "Quantum Theory of Molecules and Solids"; McGraw-Hill: New York, 1974; Vol. 4.
(18) Danese, J. B.; Connolly, J. W. D. *J. Chem. Phys.* **1974**, *61*, 3063.
(19) Stomberg, R. *Acta Chem. Scand.* **1969**, *23*, 2755.

0020-1669/84/1323-4571$01.50/0

Table II. Upper Valence Ground-State Energy Levels (eV) and Charge Distribution for $[Cr(O_2)_4]^{3-}$ [a]

				charge distrib,[b] %								
				Cr			O_1		O_2			
orbital	occupancy	type	energy	s	p	d	s	p	s	p	IS	OS
$7b_2$	0	Cr 3d	−1.88			67		20	1	2	6	4
$7a_1$	0	Cr 3d	−2.13			55		18		19	8	
9e	0	Cr 3d	−2.14			57		9		26	6	2
$3b_1$	1	Cr 3d	−4.16			84		7		2	6	1
$2b_1$	2	$\pi_g(\perp)$	−5.36			1		32		50	17	
8e	4	$\pi_g(\perp)$	−5.44			2		40		41	15	2
$2a_2$	2	$\pi_g(\perp)$	−5.54					50		31	18	1
7e	4	$\pi_g(\parallel)$	−6.61		1	18		59		7	12	3
$6b_2$	2	$\pi_g(\parallel)$	−6.72		4	7		26		45	18	
$6a_1$	2	$\pi_g(\parallel)$	−7.36			35		30		24	10	1
$1a_2$	2	$\pi_u(\perp)$	−8.45					33		50	16	1
6e	4	$\pi_u(\parallel)$	−9.01		1	12		24		52	10	1
5e	4	$\pi_u(\perp)$	−9.58		3			39		37	18	3
$5b_2$	2	$\pi_u(\parallel)$	−9.88		1	16		36		36	8	3
$5a_1$	2	$\pi_u(\parallel)$	−10.30	8			1	35	1	39	12	4
$1b_1$	2	$\pi_u(\perp)$	−10.30			10		37		29	22	2
4e	4	σ_g	−10.82		1	3	1	38	3	46	6	2
$4b_2$	2	σ_g	−11.01			5	3	42	2	41	5	2
$4a_1$	2	σ_g	−11.24			3	2	41		43	10	1
3e	4	σ_u	−19.54			1	44	3	39	3	9	1
$3a_1$	2	σ_u	−19.75			2	41	2	41	4	9	1
$3b_2$	2	σ_u	−19.88		1		43	3	37	4	11	1
2e	4	σ_g	−25.66		1	1	43	4	46	4		1
$2b_2$	2	σ_g	−25.72		1	2	41	5	46	4		1
$2a_1$	2	σ_g	−26.10	3			43	4	45	4	1	

[a] The O_1 and O_2 charge distributions refer to the charge contained in all the respective spheres of the same type. [b] The analysis of charge distribution inside atomic spheres is made according to angular momentum contributions to the total charge inside these spheres.

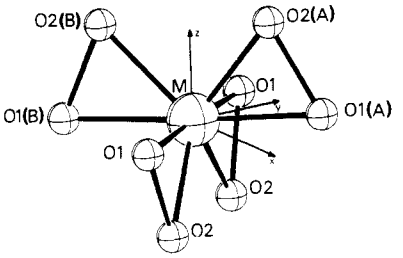

Figure 1. Structure of the $[M(O_2)_4]^{n-}$ complex.

$Cr-O_1 = 1.958$ Å, $Cr-O_2 = 1.882$ Å, $O_1-Cr-O_2 = 44.83°$, $O_1(A)-Cr-O_1(B) = 175.37°$, $O_2(A)-Cr-O_2(B) = 85.71°$; $Mo-O_1 = 2.000$ Å, $Mo-O_2 = 1.930$ Å, $O_1-Mo-O_2 = 46.30°$, $O_1(A)-Mo-O_1(B) = 177.20°$, $O_2(A)-Mo-O_2(B) = 84.70°$; $Nb-O_1 = 2.043$ Å, $Nb-O_2 = 2.008$ Å, $O_1-Nb-O_2 = 43.45°$, $O_1(A)-Nb-O_1(B) = 173.20°$, $O_2(A)-Nb-O_2(B) = 86.30°$.

Table I presents the SCF–MS–Xα calculation parameters used. The atomic exchange parameters α are taken from the calculations of Schwarz,[21,22] whereas a weighted average (based on the number of atoms) of the atomic values was chosen for the α value in the interatomic (inner-sphere) and extramolecular (outer-sphere) regions.

Overlapping atomic sphere radii were obtained nonempirically,[23] as 90% of the atomic number radii. In each case, an externally tangential outer sphere was used. In all the calculations, the electron deformation densities excepted, partial waves up to $l = 3$ were included in the multiple scattering expansions in the extramolecular region, up to $l = 2$ for the metal sphere and up to $l = 1$ in oxygen spheres. For a reliable prediction of electron deformation density distributions, previous studies have shown that this basis set must be substantially extended.[24,25] For the calculation of the density deformation of $[Cr(O_2)_4]^{3-}$, we therefore used the following maximum values: $l =$ 5 in the extramolecular region, $l = 4$ in the metal sphere, and $l = 3$ in oxygen spheres.

A Watson sphere of the same radius as the outer sphere and bearing a charge of 3+ for $[Cr(O_2)_4]^{3-}$ and $[Nb(O_2)_4]^{3-}$ and a charge of 2+ for $[Mo(O_2)_4]^{2-}$ was used in the calculations to simulate the effect of an external stabilizing electrostatic field.

The transition-state method[26] was used for the determination of excitation energies. Most of the calculations were performed by using the standard non-spin-polarized version of the SCF–MS–Xα computer programs. The only exception was the determination of the hyperfine tensor of $[Cr(O_2)_4]^{3-}$ where we used the spin-polarized version.

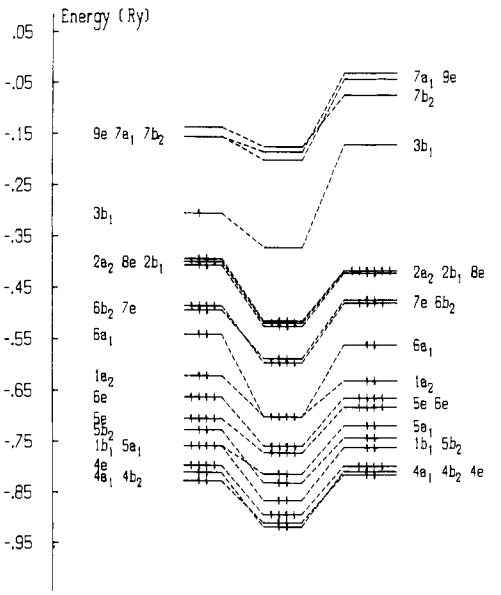

Figure 2. Upper valence ground-state energy levels for $[Cr(O_2)_4]^{3-}$ (left), $[Mo(O_2)_4]^{2-}$ (center), and $[Nb(O_2)_4]^{3-}$ (right). The electrons are depicted by arrows.

(20) Mathern, G.; Weiss, R. *Acta Crystallogr., Sect. B: Struct. Crystallogr. Cryst. Chem.* **1971**, *B27*, 1598.
(21) Schwarz, K. *Phys. Rev. B: Solid State* **1972**, *B5*, 2466.
(22) Schwarz, K. *Theor. Chim. Acta* **1974**, *34*, 225.
(23) Norman, J. G. *Mol. Phys.* **1976**, *31*, 1191.
(24) Salahub, D. R.; Foti, A. E.; Smith, V. H. *J. Am. Chem. Soc.* **1977**, *99*, 8067.
(25) Roch, M., unpublished results.
(26) Slater, J. C. *Adv. Quantum Chem.* **1972**, *6*, 1.

Table III. Upper Valence Ground-State Energy Levels (eV) and Charge Distribution for $[Mo(O_2)_4]^{2-}$ [a]

				charge distribn,[b] %								
				Mo			O_1		O_2			
orbital	occupancy	type	energy	s	p	d	s	p	s	p	IS	OS
$7b_2$	0	σ_u	−2.41			5	2	27	6	26	22	12
9e	0	Mo 4d + π_g	−2.54			36	1	20		30	11	2
$7a_1$	0	π_g + Mo 4d	−2.76			28		25		31	15	1
$3b_1$	0	Mo 4d	−5.07			72		14		4	9	1
$2b_1$	2	$\pi_g(\perp)$	−7.01			1		32		52	15	
8e	4	$\pi_g(\perp)$	−7.06			1		43		41	14	1
$2a_2$	2	$\pi_g(\perp)$	−7.15					53		30	16	1
$6b_2$	2	$\pi_g(\parallel)$	−8.00		5	3		21		56	15	
7e	4	$\pi_g(\parallel)$	−8.11		2	7		75		2	12	2
$1a_2$	2	$\pi_u(\perp)$	−9.52					32		52	15	1
$6a_1$	2	$\pi_g(\parallel)$	−9.54			29		36	1	25	9	
6e	4	$\pi_u(\perp)$	−10.32		3	3		35		43	14	2
5e	4	$\pi_u(\parallel)$	−10.49			11	1	25		52	11	
$5a_1$	2	$\pi_u(\parallel)$	−11.06	9				34		44	10	3
$5b_2$	2	σ_g	−11.30			9		42		39	9	1
$1b_1$	2	$\pi_u(\perp)$	−11.76			17		34		27	21	1
4e	4	σ_g	−12.15			13		27	3	48	7	2
$4a_1$	2	σ_g	−12.37			8	3	39		40	9	1
$4b_2$	2	$\pi_u(\parallel)$	−12.48			19	4	41	1	29	3	3
3e	4	σ_u	−21.32			2	49	2	37	2	7	1
$3b_2$	2	σ_u	−21.44		1	1	41	2	42	3	9	1
$3a_1$	2	σ_u	−21.58			3	42	2	41	3	8	1
2e	4	σ_g	−26.10		3	2	39	3	48	3	1	1
$2b_2$	2	σ_g	−26.46		2	4	44	3	43	3		1
$2a_1$	2	σ_g	−26.61	3			42	3	45	3	3	1

[a] The O_1 and O_2 charge distributions refer to the charge contained in all the respective spheres of the same type. [b] The analysis of charge distribution inside atomic spheres is made according to angular momentum contributions to the total charge inside these spheres.

Table IV. Upper Valence Ground-State Energy Levels (eV) and Charge Distribution for $[Nb(O_2)_4]^{3-}$ [a]

				charge distribn,[b] %								
				Nb			O_1		O_2			
orbital	occupancy	type	energy	s	p	d	s	p	s	p	IS	OS
9e	0	Nb 4d + π_g	−0.45			33	2	15		20	13	17
$7a_1$	0	π_g + Nb 4d	−0.61			21	2	21	1	27	19	9
$7b_2$	0	σ_u	−1.03		1		2	14	6	11	27	39
$3b_1$	0	Nb 4d	−2.35			76		9		2	11	2
8e	4	$\pi_g(\perp)$	−5.68			1		41		41	15	2
$2b_1$	2	$\pi_g(\perp)$	−5.68					31		51	18	
$2a_2$	2	$\pi_g(\perp)$	−5.75					49		33	17	1
$6b_2$	2	$\pi_g(\parallel)$	−6.45		4	3		21		53	18	1
7e	4	$\pi_g(\parallel)$	−6.54		1	9		65		9	13	3
$6a_1$	2	$\pi_g(\parallel)$	−7.64			25		31		32	11	1
$1a_2$	2	$\pi_u(\perp)$	−8.58					34		48	17	1
6e	4	$\pi_u(\parallel)$	−9.03		3	9		25		51	9	3
5e	4	$\pi_u(\perp)$	−9.28		1	1		35		42	19	2
$5a_1$	2	$\pi_u(\parallel)$	−9.76	8				39		38	11	4
$5b_2$	2	$\pi_u(\parallel)$	−10.09		1	13		44		32	8	2
$1b_1$	2	$\pi_u(\perp)$	−10.35			10		37		28	23	2
4e	4	σ_g	−10.84			5	1	37	3	45	7	2
$4b_2$	2	σ_g	−10.98			7	3	44	1	37	5	3
$4a_1$	2	σ_g	−11.07			3	2	42		42	10	1
3e	4	σ_u	−19.81			1	45	3	38	3	9	1
$3b_2$	2	σ_u	−19.90		1	1	39	3	43	3	10	
$3a_1$	2	σ_u	−20.04			2	41	2	41	4	9	1
2e	4	σ_g	−25.09		5	1	39	4	47	3		1
$2b_2$	2	σ_g	−25.46		2	3	45	4	41	4		1
$2a_1$	2	σ_g	−25.61	3			44	3	45	3	1	1

[a] The O_1 and O_2 charge distributions refer to the charge contained in all the respective spheres of the same type. [b] The analysis of charge distribution inside atomic spheres is made according to angular momentum contributions to the total charge inside these spheres.

Results and Discussion

Ground-State Electronic Structures. The ground-state electronic structures of $[Cr(O_2)_4]^{3-}$, $[Mo(O_2)_4]^{2-}$, and $[Nb(O_2)_4]^{3-}$ are presented in Tables II–IV and compared graphically in Figure 2.

There are some similarities in the ordering of the occupied valence and virtual MOs for the three complexes: the low-lying virtual MOs are of predominant metal character, with the result that the mostly metal *d* orbital $3b_1$ is the HOMO for the d^1 Cr(V) complex and the LUMO for the d^0 Mo(VI) and Nb(VI) compounds. This leads to the following ground-state configurations:[27]

$$[Cr(O_2)_4]^{3-}: \ ^2B_1\ (2a_2)^2(8e)^4(2b_1)^2(3b_1)^1$$

$$[Mo(O_2)_4]^{2-}: \ ^1A_1\ (2a_2)^2(8e)^4(2b_1)^2$$

$$[Nb(O_2)_4]^{3-}: \ ^1A_1\ (2a_2)^2(2b_1)^2(8e)^4$$

Table V. Metal Configuration in the Peroxo Complexes

complex	electron population on metal[a]								metal charge
			*n*d						
	$(n+1)$s	$(n+1)$p	z^2	x^2-y^2	xy	xz	yz	total	
$[Cr(O_2)_4]^{3-}$	0.22	0.46	0.80	1.06	0.60	0.72	0.72	3.90	1.42+
$[Mo(O_2)_4]^{2-}$	0.24	0.48	0.80	0.36	0.72	0.78	0.78	3.44	1.84+
$[Nb(O_2)_4]^{3-}$	0.22	0.56	0.60	0.20	0.54	0.54	0.54	2.42	1.80+

[a] The electron population of metal atomic orbitals has been obtained by summing up over *all* the occupied MOs of the valence shell, with the intersphere and outer-sphere charge fully attributed to ligands.

The sequence of metal d orbitals agrees with the results of crystal field theory[28] $d_{x^2-y^2}$ $(3b_1) \leq d_{z^2}$ $(7a_1) \simeq d_{xy,yz}$ $(9e) \leq d_{xy}$ $(7b_2)$, though these MOs, $3b_1$ excepted, exhibit considerable differences in their charge distributions when going from the Cr to the Mo and Nb complexes. In all three complexes the $3b_1$ MO is strongly localized on the metal and appears to be essentially nonbonding, as might be expected (it lies in the equatorial plane and has maximum density in between the oxygen atoms).

For a better understanding of the metal dioxygen interaction, we may discuss the structure in terms of the interaction between a metal ion and four peroxides and recall that the peroxide ion O_2^{2-} has the following ground-state configuration: $(2\sigma_g)^2(2\sigma_u)^2(3\sigma_g)^2(1\pi_u)^4(1\pi_g)^4$.[1] In η^2 triangular coordination of the metal atom by the peroxide, the π_g and π_u MOs of the ligands split into components $\pi_g(\parallel)$ and $\pi_u(\parallel)$, lying essentially in the MO_2 plane, and $\pi_g(\perp)$ and $\pi_u(\perp)$ perpendicular to this plane. For the $[M(O_2)_4]^{n-}$ complexes in D_{2d} symmetry, the ligand π MOs of $\parallel$ type belong to the a_1, b_2, and e symmetries, whereas those of $\perp$ type belong to a_2, b_1, and e. It is thus not possible to determine by symmetry alone the nature of ligand e levels since they are generally mixtures of both $\parallel$ and $\perp$ contributions. In practice, however, we find by inspection of the orbitals that the ligand-based orbitals may readily be associated with one of the MOs of the peroxide ion, and in the following discussion we will classify these levels according to their main component.

Examination of Tables II–IV and of Figure 2 indicates that in all the complexes the nonbonding levels $2a_2$, 8e, and $2b_1$, which are all of $\pi_g(\perp)$ type, are the highest occupied MOs, $2b_1$ being the HOMO in the Mo case whereas 8e is the HOMO of tetraperoxoniobate. The charge distribution resulting from these MOs is on average equally shared by the two oxygen atoms, and the amount of residual charge on the metal is, as expected, negligible. Below the $\pi_g(\perp)$ levels, one finds, in sequence, the predominantly $\pi_g(\parallel)$ $(6a_1, 6b_2, 7e)$ and π_u $(1b_1, 5a_1, 5b_2, 5e, 6e, 1a_2)$ orbitals of the ligands. But, whereas these two groups of levels are well separated in energy in the Cr and Nb cases, the $\pi_g(\parallel)$ family lying above the π_u one, they are mixed together in the Mo case, the $6a_1$ MO of $\pi_g(\parallel)$ type being located below $1a_2$ of π_u character. The $\pi_g(\parallel)$-based MOs are all bonding and exhibit a large covalent mixing with metal d orbitals. This is especially true for the $6a_1$ MO, which is quite strongly bonding in all the complexes, resulting from a considerable in-phase admixture of the d_{z^2} orbital of metal to the in-plane π_g level of the ligand O_2^{2-} (Figure 3).

The π_u-based MOs, though lying generally at significantly lower energies than the levels with predominant $\pi_g(\parallel)$ character, also show a substantial interaction with the metal orbitals. For all these complexes, the separation between $\pi_u(\perp)$ and $\pi_u(\parallel)$ levels is much less clear-cut than that between $\pi_g(\parallel)$ and $\pi_g(\perp)$, and both types of levels are mixed together within the π_u band. In contrast to the π_g MOs, the π_u levels exhibiting the largest admixture of metal d orbitals are of both $\perp$ type $(1b_1)$ and $\parallel$ type $(5b_2, 5e, 6e)$. Finally, the lower lying valence levels $4a_1$, $4b_2$, and 4e are essentially O–O σ_g bonding in character and show little interaction with the metal in the Cr and Nb cases. It is to be noticed that in the Mo complex, the σ_g and π_u orbitals are mixed together and are more involved in metal–ligand bonding as exemplified by their larger charge distribution on the metal. At lower energies, one finds, in sequence, the series of ligand levels originating from the $2\sigma_u$ and $2\sigma_g$ orbitals of peroxide. They are typically ligand-based levels and show a negligible interaction with the metal. As to the virtual orbitals, we have already noticed that the $7a_1$, 9e, and $7b_2$ MOs are significantly modified when going from Cr to Mo and Nb complexes: their delocalization over the oxygen atoms increases along this series, and they show considerable O–O antibonding character for molybdate and niobate. As a result of the higher oxidation state of the metal in $[Mo(O_2)_4]^{2-}$, these orbitals lie at much lower energies. It is clear that the bonding of peroxide to the highest oxidation state metal (Mo(VI)) leads to a much greater disruption of the electronic structure and may therefore be of greater effect in activating the peroxide species.

The $M–O_1$ and $M–O_2$ distances in the Cr(V) and Mo(VI) complexes are significantly different (by nearly 0.1 Å), and it is interesting to seek an explanation for this distortion in the results of our calculations. Although the symmetry of the complex does not require the two M–O distances to be equal, symmetric coordination of η^2 dioxygen is generally found in most other known complexes. To simplify the discussion, we will consider here only the interactions in the MO_2 plane that have been shown above to be the most important. Examination of Table II shows that for the Cr(V) complex there are four MOs with important admixtures of metal 3d orbitals into $\pi_g(\parallel)$ or $\pi_u(\parallel)$ levels of ligands: 7e, $6a_1$, 6e, $5b_2$. As may be seen from Figure 3, the $6a_1$ and the $5b_2$ MOs exhibit very similar $M–O_1$ and $M–O_2$ bonding interactions, and this is confirmed by the nearly equal O_1 and O_2 characters presented by each of these MOs. The 7e and 6e levels, however, reveal strong differences in their O_1 vs. O_2 contributions: 7e has 59% O_1 and 7% O_2 character, and the corresponding figures for 6e are 24% and 52%. In addition, inspection of Figure 3 indicates that for both 7e and 6e the metal–O_2 interactions are strongly σ bonding whereas the metal–O_1 interaction is weakly σ bonding for 7e and π antibonding for 6e. The net balance of these interactions is thus undoubtedly in favor of stronger metal–O_2 bonding interactions than metal–O_1 ones, which leads in turn to a $Cr–O_2$ bond distance smaller than $Cr–O_1$. The same qualitative arguments would also apply for the Mo(VI) and Nb(V) complexes, though to a lesser extent for the latter since the difference between $Nb–O_1$ and $Nb–O_2$ distances is smaller.

Table V presents the electronic configuration of the metal in the three complexes. It is seen that the $(n+1)$s and $(n+1)$p populations do not undergo great changes along the series Cr, Mo, and Nb and remain rather small, which indicates that the role of these orbitals in the bonding of the complexes is

(27) In all cases, only the valence MOs are labeled and numbered according to the irreducible representations of the D_{2d} symmetry group.
(28) Swalen, J. D.; Ibers, J. A. *J. Chem. Phys.* **1962**, *37*, 17.

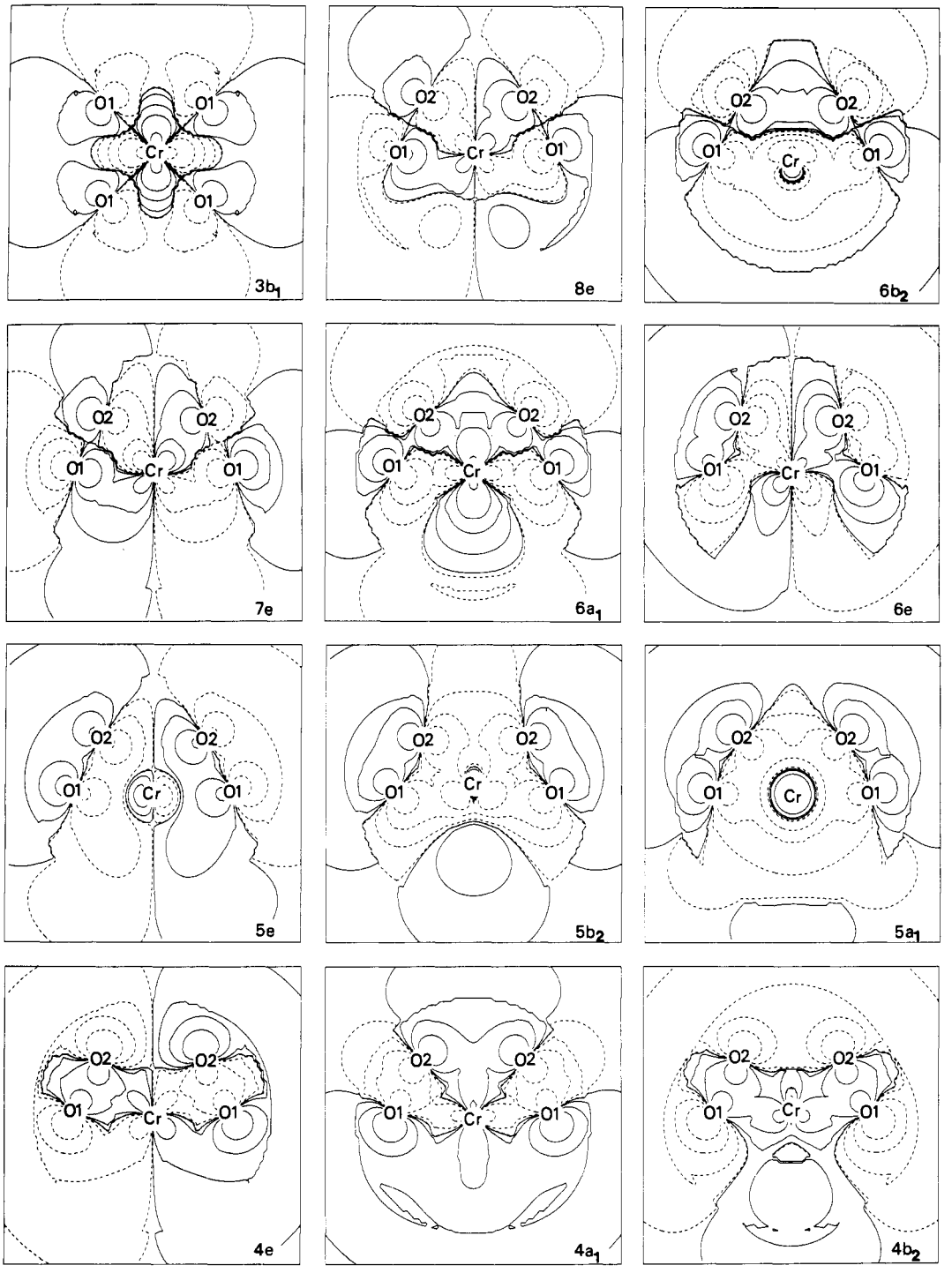

Figure 3. Wave function contours of some important MOs of $[Cr(O_2)_4]^{3-}$. Except for $3b_1$, which is plotted in the x, 0, y plane, all the MOs are represented in the 1, 1, 0 vertical plane containing two MO_2 units. Positive wave function contours are indicated by a solid line while negative contours are represented by a dashed line.

not important. Actually the Xα result confirms the assumption, based on qualitative and intuitive reasoning, that the (n + 1)s and (n + 1)p orbitals of the metal interact only weakly with the π_g levels of the ligands in peroxides in view of their large energy separation from the predominantly nd MOs.[4] Our conclusion is also in agreement with the data available for the d^{10} complex zinc tetraphenylporphyrin superoxide,[29] where any covalent bonding must involve the 4s and 4p orbitals: it was concluded that the bonding is essentially ionic and the complex is not particularly stable, arguing for a small role of the 4p orbitals. We find a small amount of d–p mixing in some bonding orbitals (6e, 7e, $6b_2$) of the Cr, Mo, and Nb tetraperoxides (Tables II–IV), in agreement with the MS–Xα results of Norman and Ryan[12] for $M(PH_3)_4(O_2)^+$ (M = Co, Rh, Ir) that show that d–p hybridization might play some role in M–O bonding in peroxo complexes with phosphine ligands.

Examination of Table V indicates that the population of metal d orbitals is considerable in all cases, underlining the large degree of covalent interaction between metal d and ligand π_g orbitals. Indeed, taking into account that the predominantly 3d LUMO of the Cr complex has an intrinsic charge of 0.84e in the metal sphere, the ligand to metal nd charge-transfer donation amounts to 3.06e, 3.44e, and 2.42e in Cr, Mo, and Nb complexes, respectively. As expected, the higher oxidation state of the metal in the molybdenum complex as compared

(29) Valentine, J. S.; Tatsuno, Y.; Nappa, M. *J. Am. Chem. Soc.* **1977**, *99*, 3522.

Table VI. Analysis of the Ligand-to-Metal Charge Donation in the Peroxo Complexes[a]

charge donation	Cr		Mo		Nb	
	⊥	∥	⊥	∥	⊥	∥
$\sigma_g \rightarrow n$d		0.32		1.02		0.50
$(n+1)$s		0.06		0.06		0.06
$(n+1)$p		0.14		0.16		0.24
total		0.52		1.24		0.80
$\sigma_u \rightarrow n$d		0.08		0.16		0.10
$(n+1)$p		0.02		0.02		0.02
total		0.10		0.18		0.12
$\pi_g \rightarrow n$d	0.10	1.56	0.06	0.92	0.04	0.92
$(n+1)$p		0.12		0.18		0.12
total	0.10	1.68	0.06	1.10	0.04	1.04
$\pi_u \rightarrow n$d	0.20	0.80	0.46	0.82	0.24	0.62
$(n+1)$s		0.16		0.18		0.16
$(n+1)$p	0.12	0.06	0.12		0.04	0.14
total	0.32	1.02	0.58	1.00	0.28	0.92

[a] Analysis performed with the same conventions as in Table V. For an explanation of the symbols, see text.

with the chromium and niobium complexes leads to the largest ligand to metal donation for this compound. Comparing the corresponding values obtained for the Cr and Nb complexes, it is natural that the former exhibits a larger ligand to metal donation since it is established that the 3d orbital of atomic chromium lies at a lower energy (−6.52 eV) than the 4d orbital of niobium (−6.10 eV).[30] Finally, it is interesting to notice that the difference in ligand to metal donation between the isoelectronic $[Mo(O_2)_4]^{2-}$ and $[Nb(O_2)_4]^{3-}$ complexes is almost exactly equal to the difference of the oxidation numbers of the metal atoms (+1.02 instead of +1.0), which leads of course to very similar metal charges in both compounds. This is a very good illustration of the very loose relation between oxidation numbers and atomic charges in coordination chemistry.[31]

In order to evaluate in more detail the mechanism of ligand to metal charge-transfer donation, Table VI presents for the three complexes an analysis of the charge transferred by each type of predominantly ligand MOs. It is seen that whereas the MOs perpendicular to the MO_2 planes (⊥) play a very minor role in π_g bonding, they are much more delocalized onto the metal in the case of π_u orbitals. This is mostly due to the bonding nature of the $\pi_u(\perp)$ MO, $1b_1$, which is the bonding partner of the weakly antibonding $3b_1$ MO, whereas the $\pi_g(\perp)$ $2b_1$ is nonbonding. Moreover, the charges donated by the different ligand type MOs undergo considerable change along the series Cr, Mo, and Nb: whereas the contribution from the low-lying σ_u levels is small, that from the σ_g levels is far from negligible, with the Mo complex exhibiting a substantial σ_g ligand to metal donation of 1.24e, which actually makes the σ_g channel the most important source of ligand to metal charge donation for this complex. This surprising result is undoubtedly due to the higher oxidation state of the metal in this complex, which results in a smaller energy gap between the occupied levels of the ligands and the metal 4d orbitals and ultimately to a larger admixture of metal 4d character into the low-lying bonding MOs. As expected, the donation from π_g MOs is important for all the complexes, but it is the largest source of charge transfer only for the Cr compound. Indeed, surprisingly enough, the total charge donation through the π_u orbitals is not only of the same order of magnitude as that arising through the π_g MOs, but it is even larger for the Mo and Nb complexes. However, a detailed examination of Table VI reveals that when considering the in-plane ∥ components only, the transfer from π_g is larger than that arising from π_u in all cases. It is only by adding the out-of-plane ⊥ components, which are much more important for π_u than for π_g mainly because of the large admixture of metal *n*d into the $1b_1$ MO, that this trend is reversed for the Mo and Nb complexes. The difference in interaction for $\pi_u(\perp)$ and $\pi_g(\perp)$ may be rationalized by considering the symmetries of these orbitals with respect to an axis joining the metal to the center of the O–O bond. The $\pi_u(\perp)$ orbital has π symmetry with respect to this axis whereas the $\pi_g(\perp)$ has δ symmetry. But in any case, the contribution of π_u orbitals (and, for $[Mo(O_2)_4]^{2-}$, of σ_g ones as well) is of equal importance to that of π_g, and all of them should be included in a realistic description of the electronic structure of dioxygen complexes.

It is interesting to compare the amount of charge donated to the metal by the ligand MOs that are bonding for the O–O units (i.e., π_u and σ_g) with the corresponding value obtained for the O–O antibonding MOs (i.e., π_g and σ_u), in order to correlate these values with the observed O–O bond lengths in these complexes. It is seen from Table VI that the total $\sigma_g + \pi_u$ charge donation amounts to 1.86e, 2.82e, and 2.00e for the Cr, Mo, and Nb complexes, respectively, whereas corresponding values for the $\sigma_u + \pi_g$ MOs are 1.88e, 1.34e, and 1.20e. Thus, for $[Cr(O_2)_4]^{3-}$ the donation from O–O bonding orbitals almost exactly compensates that arising from antibonding ones, whereas for $[Mo(O_2)_4]^{2-}$ and $[Nb(O_2)_4]^{3-}$ the balance is in favor of a transfer from the bonding MOs by 1.48e and 0.80e, respectively. According to these figures, one would expect the O–O distance in the Cr complex to be quite close to the corresponding value observed for the peroxide ion O_2^{2-} (1.49 Å),[2] while it should be significantly larger for the Mo complex and intermediate in the case of Nb. This conclusion is in very good agreement with the structural data,[8,19,20] which lead to the following values for the O–O bond lengths: 1.466, 1.544, and 1.500 Å for the Cr, Mo, and Nb complexes, respectively. Since two of our compounds have formally a d^0 ground state, no back-donation is expected from the d orbitals of metal. Thus, the Dewar–Chatt–Duncanson synergic scheme[32] of bonding must be ruled out, and it can not be invoked, as has been done for d^8 peroxides,[33] to account for the large range of O–O distances observed for d^0 peroxides. Instead, the present results suggest that the variations of the balance between $(\sigma_g + \pi_u)$ and $(\sigma_u + \pi_g)$ ligand to metal donations are able to rationalize this structural aspect of d^0 peroxo complexes.

One extended Hückel[34] (EHMO) and two ab initio SCF[8,10] calculations have been reported for $[Cr(O_2)_4]^{3-}$. All of these calculations are essentially in agreement with the present ones in predicting a $^2B_1$ ground state for this complex and in showing that the bonding is mostly covalent, involving mainly those orbitls of dioxygen lying in the plane of the η^2 CrO_2 unit. In all these calculations and in Xα as well, the predominant contribution to metal–ligand bonding arises through the $6a_1$ MO. However, when comparing these results in greater detail, one notices some important differences. Whereas our results (85%), EHMO (60%),[34] and the ab initio calculation of Dacre and Elder (98%)[10] find the unpaired electron accommodated in the $3b_1$ MO to be essentially localized on the metal in the $3d_{x^2-y^2}$ orbital, the ab initio calculation of Fischer, Veillard, and Weiss[8] leds to a singly occupied $3b_1$ MO localized on the dioxygen ligands. Since, in addition, this surprising result is in disagreement with qualitative ligand field arguments and the interpretation of ESR measurements,[35] there is not doubt

(30) Herman, F.; Skillman, S. "Atomic Structure Calculations"; Prentice-Hall: Englewood Clills, NJ, 1963.
(31) Williams, A. F. "A Theoretical Approach to Inorganic Chemistry"; Springer-Verlag: Berlin, 1979.
(32) (a) Dewar, M. J. S. *Bull. Soc. Chim. Fr.* **1951**, *18*, C79. (b) Chatt, J.; Duncanson, L. A. *J. Chem. Soc.* **1953**, 2339.
(33) McGinnety, J. A.; Payne, N. C.; Ibers, J. *J. Am. Chem. Soc.* **1969**, *91*, 6301.
(34) Rösch, N.; Hoffmann, R. *Inorg. Chem.* **1974**, *13*, 2656.

that this assignment may be ruled out. Another source of disagreement between the calculations is concerned with the gross charge on the chromium atom: Xα (1.42+) and EHMO (1.85+) are in reasonable agreement, but the ab initio results of Dacre and Elder (0.72−) and of Fischer et al. (2.58+) disagree significantly. Though the calculation of atomic charges from the molecular wave functions is somewhat arbitrary, these results underline the importance of choosing an adequate one-electron basis set in ab initio SCF calculations. Indeed, the large difference in metal charges between the two ab initio calculations is mainly due to the role of the 4s and 4p orbitals: because of a different choice of basis functions, Dacre and Elder find these orbitals to be occupied by 3.68 electrons whereas Fischer et al. find a virtually zero occupation of these orbitals.

A semiempirical calculation, performed with the SCMO model, has been reported for $[Mo(O_2)_4]^{2-}$.[36] These results do not agree very well with the present ones since they lead to a very large energy gap (13 eV) between the HOMO (localized on the oxygen atoms) and the LUMO (localized on the metal) and to a large charge on the metal (3.38+). As no details are reported by these authors concerning the charge distribution of the MOs, any further comparison of the ground-state electronic structures between the two calculations is impossible.

SCF–MS–Xα calculations have been carried out on the d^6 systems[12] $[M(PH_3)_4(O_2)]^+$ and the d^8 system[37] $Pt(PH_3)_2O_2$. In all cases the $\pi_g(\perp)$ orbital is the highest occupied molecular orbital and is essentially nonbonding. For the group 8 metals, however, the occupied d orbitals lie below the $\pi_g(\perp)$ and for all except $[Co(PH_3)_4(O_2)]^+$ lie below the $\pi_g(\parallel)$ orbitals. There is thus an inversion of the relative energies of dioxygen π_g and metal d orbitals between the group 5 and 6 metals studied here and the group 8 metals studied by Norman and Ryan. In the latter systems the interaction of the occupied π_u orbitals is primarily with the filled metal d orbitals and has a negligible effect on the bonding.

Reactivity. Complexes formed by d^0 metal ions with hydrogen peroxide or alkyl hydroperoxides are frequently efficient catalysts for the epoxidation of alkenes. Mimoun has shown that the η^2 dioxygen complex of Mo(VI), $MoO(O_2)_2HMPT$, is an efficient catalyst for epoxidation.[38] η^2 dioxygen complexes of Ti(IV) are however inert,[39] and Ti(IV)[40] and V(V)[41] apparently epoxidize alkenes via hydroperoxide or alkyl peroxide intermediates. Mimoun has recently differentiated clearly the pathways for epoxidation involving peroxides and hydroperoxides.[42]

Our calculations give some indications as to the uniquely efficient epoxidation properties of the group 6 d^0 peroxides. We have shown that it is in the molybdenum complex that the O–O bond is the most weakened and that there is the maximum mixing between the d orbitals and the peroxide orbitals. Furthermore, the negative charge on the oxygen atoms is lower in the molybdenum complex (and would be expected to be lower still in the catalytically active complexes that are neutral), and the low-lying virtual orbitals show appreciable O–O σ-antibonding character. These features would favor reactions involving nucleophilic attack on the dioxygen followed by cleavage of the O–O bond, as required for epoxidation. It is known that the dioxygen in Mo(VI) complexes shows some electrophilic character[43] and that the most nucleophilic alkenes are the most readily epoxidized.[44] In the case of the Nb(V) complex, the O–O bond is less weakened and the negative charge on the oxygen atoms is greater. Nucleophilic attack on the dioxygen ligand is thus less favored, while protonation to give a hydroperoxide is more favored. As mentioned above, the complexes of V(V) appear to react via a hydroperoxide intermediate.[41]

Table VII. Calculated[a] Electronic Excitation Energies (cm^{-1}) of $[Cr(O_2)_4]^{3-}$

transition	type of transition[b]	calcd value
$8e \rightarrow 3b_1$	$\pi_g(\perp) \rightarrow 3d$	14 500
$2a_2 \rightarrow 3b_1$		15 600
$3b_1 \rightarrow 9e$	$d \rightarrow d$	16 700
$7e \rightarrow 3b_1$	$\pi_g(\parallel) \rightarrow 3d$	22 900
$2b_1 \rightarrow 9e$	$\pi_g(\perp) \rightarrow 3d$	28 200
$8e \rightarrow 7a_1$		28 700
$8e \rightarrow 9e$		28 700
$2a_2 \rightarrow 9e$		29 800
$8e \rightarrow 7b_2$		31 500
$7e \rightarrow 7a_1$	$\pi_g(\parallel) \rightarrow 3d$	37 600
$7e \rightarrow 9e$		37 800
$6b_2 \rightarrow 9e$		38 600
$6b_2 \rightarrow 7a_1$		38 700
$7e \rightarrow 7b_2$		40 100

[a] Non-spin-polarized calculations. Orbitally allowed transitions only are reported. [b] $3b_1 \rightarrow 9e$ excepted, all the transitions are of ligand-to-metal charge-transfer type.

Table VIII. Calculated[a] Electronic Excitation Energies (cm^{-1}) of $[Mo(O_2)_4]^{2-}$

transition	type of transition[b]	calcd value
$8e \rightarrow 3b_1$	$\pi_g(\perp) \rightarrow 4d$	19 800
$2a_2 \rightarrow 3b_1$		20 700
$7e \rightarrow 3b_1$	$\pi_g(\parallel) \rightarrow 4d$	28 100
$8e \rightarrow 7a_1$	$\pi_g(\perp) \rightarrow \pi_g(\parallel) + 4d$[c]	35 200
$2b_1 \rightarrow 9e$	$\pi_g(\perp) \rightarrow 4d + \pi_g(\parallel)$[c]	36 900
$8e \rightarrow 9e$		37 300
$8e \rightarrow 7b_2$	$\pi_g(\perp) \rightarrow \sigma_u$	37 600
$2a_2 \rightarrow 9e$	$\pi_g(\perp) \rightarrow 4d + \pi_g(\parallel)$[c]	38 100
$1a_2 \rightarrow 3b_1$	$\pi_u(\perp) \rightarrow 4d$	39 800
$6b_2 \rightarrow 7a_1$	$\pi_g(\parallel) \rightarrow \pi_g(\parallel) + 4d$[c]	42 700
$7e \rightarrow 7a_1$		44 200
$6b_2 \rightarrow 9e$	$\pi_g(\parallel) \rightarrow 4d + \pi_g(\parallel)$[c]	44 700
$7e \rightarrow 9e$		46 300
$7e \rightarrow 7b_2$	$\pi_g(\parallel) \rightarrow \sigma_u$	46 800

[a] Non-spin-polarized calculations. Orbitally allowed transitions only are reported. [b] All the transitions reported are either of ligand-to-metal or ligand-to-ligand charge-transfer type. [c] Owing to the large mixing of the virtual MO, this transition cannot be unambiguously assigned to a definite type.

Electronic Absorption Spectra. The tetraperoxochromate and -molybdate ions are dark red, and the tetraperoxoniobate is colorless. More precise data are lacking as all these compounds are unstable in aqueous solution, either losing hydrogen peroxide or being protonated. Such data as have been reported are somewhat contradictory, presumably as a result of partial decomposition. For $[Cr(O_2)_4]^{3-}$ there is a band near 20 000 cm^{-1},[28,45,46] with a molar extinction coefficient between 50 and

(35) Dalal, N. S.; Millar, J. M.; Jagadeesh, M. S.; Seehra, M. S. *J. Chem. Phys.* **1981**, *74*, 1916.
(36) Brown, D. H.; Perkins, P. G. *Inorg. Chim. Acta* **1974**, *8*, 285.
(37) Norman, J. G. *Inorg. Chem.* **1977**, *16*, 1328.
(38) Mimoun, H.; Serée de Roch, I.; Sajus, L. *Tetrahedron* **1960**, *26*, 37.
(39) Mimoun, H.; Postel, M.; Casabianca, F.; Fischer, J.; Mitschler, A. *Inorg. Chem.* **1982**, *21*, 1303.
(40) Rossiter, B. E.; Katsuki, T.; Sharpless, K. B. *J. Am. Chem. Soc.* **1981**, *103*, 464.
(41) Mimoun, H.; Saussine, L.; Daire, E.; Postel, M.; Fischer, J.; Weiss, R. *J. Am. Chem. Soc.* **1983**, *105*, 3101.
(42) Chaumette, P.; Mimoun, H.; Saussine, L.; Fischer, J.; Mitschler, A. *J. Organomet. Chem.* **1983**, *250*, 291.
(43) Regen, S. L.; Whitesides, G. M. *J. Organomet. Chem.* **1973**, *59*, 293.
(44) Sharpless, K. B.; Townsend, J. M.; Williams, D. R. *J. Am. Chem. Soc.* **1972**, *94*, 295.
(45) McGarvey, B. R. *J. Chem. Phys.* **1962**, *37*, 2001.
(46) Gubelmann, M.; Williams, A. F., unpublished data.

Table IX. Calculated[a] Electronic Excitation Energies (cm^{-1}) of $[Nb(O_2)_4]^{3-}$

transition	type of transition[b]	calcd value
$8e \rightarrow 3b_1$	$\pi_g(\perp) \rightarrow 4d$	31 700
$2a_2 \rightarrow 3b_1$		32 500
$7e \rightarrow 3b_1$	$\pi_g(\parallel) \rightarrow 4d$	38 100
$8e \rightarrow 7b_2$	$\pi_g(\perp) \rightarrow \sigma_u$	38 200
$8e \rightarrow 7a_1$	$\pi_g(\perp) \rightarrow \pi_g(\parallel) + 4d$[c]	41 200
$8e \rightarrow 9e$	$\pi_g(\perp) \rightarrow 4d + \pi_g(\parallel)$[c]	42 900
$2b_1 \rightarrow 9e$		43 000
$2a_2 \rightarrow 9e$		43 500
$7e \rightarrow 7b_2$	$\pi_g(\parallel) \rightarrow \sigma_u$	45 600
$6b_2 \rightarrow 7a_1$	$\pi_g(\parallel) \rightarrow \pi_g(\parallel) + 4d$[c]	47 400
$7e \rightarrow 7a_1$		48 500
$6b_2 \rightarrow 9e$	$\pi_g(\parallel) \rightarrow 4d + \pi_g(\parallel)$[c]	49 000

[a] Non-spin-polarized calculations. Orbitally allowed transitions only are reported. [b] All the transitions reported are either of ligand-to-metal or ligand-to-ligand charge-transfer type. [c] Owing to the large mixing of the virtual MO, this transition cannot be unambiguously assigned to a definite type.

500, and a second band near 27 000 cm^{-1}.[45,46] For $[Mo(O_2)_4]^{2-}$ the spectrum shows absorption rising steadily to 44 000 cm^{-1},[36] although other workers have observed weak features at 22 000 and 32 000 cm^{-1}.[45]

In view of the rather poor resolution of the experimental spectra, we performed non-spin-polarized transition-state calculations in order to estimate the energy values and the corresponding assignments of the electronic transitions in the three complexes (Tables VII–IX). These calculations are of semiquantitative value only, since it is well-known that spin-polarized calculations would actually split up the different spin multiplets resulting from each excited configuration and thus account partly for multiplet structure effects. However, these calculations would require a prohibitive amount of computer time without changing qualitatively our interpretation of the spectra. As an example, let us mention that in the Cr(V) case the lowest (doublet to doublet) transitions involving excitations into a metal 3d level would be predicted to lie at slightly higher energies in the spin-polarized model because a larger exchange splitting may be expected for the d-like final state. Similarly, in some other cases, the present calculations underestimate the transition energies because of the neglect of the singlet–triplet splittings.

As has been suggested[3] the majority of the low-energy transitions are ligand-to-metal charge transfer (LMCT) in character. The lowest energy transitions are $\pi^*(\perp)-3b_1$ ($d_{x^2-y^2}$) in all three cases; as these are transitions from orbitals perpendicular to the xy plane into the xy plane, they would be expected to be weak[3] and this is supported by preliminary calculations of their intensity.[47] Although the experimental molar extinction coefficients are not known with any precision, they do appear to be less than 10^3 L mol^{-1} cm^{-1}, in agreement with this. The lowest energy bands are at 14 500, 19 800, and 31 700 cm^{-1} for the chromium, molybdenum, and niobium complexes. Although the calculated energies are rather lower than the first observed bands for the chromium and molybdenum complexes, the order Cr ≤ Mo ≤ Nb is indeed that which is observed, and $[Nb(O_2)_4]^{3-}$ is predicted to be colorless.

The d–d transition in $[Cr(O_2)_4]^{3-}$ is calculated to lie above the lowest charge-transfer bands. All the complexes show a succession of LMCT bands at steadily increasing energies. In many cases these involve transitions between orbitals localized in different planes and would be expected to be weak. It is only in the upper end of the spectrum that transitions between the bonding $\pi_g(\parallel)$ and antibonding d orbitals (which would be expected to have high intensity) may be observed.

(47) Weber, J.; Roch, M.; Goursot, A., to be submitted for publication.

Theoretical Electron-Deformation Density Distribution in $[Cr(O_2)_4]^{3-}$. It is well-known that the distribution of electron densities in molecules and molecular solids can now be accurately measured by experimental techniques such as X-ray and neutron scattering.[48,49] This information is presented as maps of electron-deformation density distribution, i.e. contour maps of the difference $\Delta\rho(r)$ between a molecular electronic density distribution and the superposition of spherically averaged atomic distributions. Since core electrons are relatively unperturbed by the chemical environment, this function $\Delta\rho(r)$ represents the deformation that occurs in valence electron density when the atoms interact to form chemical bonds. Of course, the nature of the deformation density, and ultimately the description of bond formation, depends largely on the particular choice of atomic densities used (i.e., the nature of the so-called promolecule),[50] and this is particularly true for a compound such as $[Cr(O_2)_4]^{3-}$ where there are different ways to distribute the excess charge of 3e among the atoms of the promolecule.

The incentive to perform such a calculation for $[Cr(O_2)_4]^{3-}$ was the following: (i) only a few MS–Xα studies of electron density distributions have appeared for a series of first- and second-row homonuclear diatomics[50,51] and for S_8;[24] the present study is thus the first application of the MS–Xα model to the calculation of the deformation density in a coordination compound; (ii) an experimental determination of the electron-deformation density in K_3CrO_8 is in progress,[52] which will provide an interesting comparison with the present results, leading ultimately to a severe test of the quality of our wave functions. In particular, it could be useful to evaluate the importance of the muffin-tin approximation inherent in the MS–Xα model by comparing in detail the theoretical electron-deformation map with the experimental one, inasmuch as previous calculations performed in this Laboratory have shown this approximation to be of little importance for the prediction of several electronic observables.[13,14] In addition, we should mention that to our knowledge very few theoretical determinations of electron-deformation maps, using other computational models, have been reported for coordination compounds,[53,54] and the present results should indicate whether Xα could play a significant role in this field.

As mentioned in the Calculations, the partial-wave basis set was significantly extended for this particular calculation. Contrary to the previous Xα investigations,[24,50,51] the frozen-core approximation was not used in the present calculations. Instead, the density distribution of core electrons was allowed to relax during the SCF procedure,[55] and in order to represent the deformation density of valence electrons only, the molecular electron density was calculated as the sum over contributions from all the levels listed in Table II, i.e. those exhibiting contributions from 3d, 4s, and 4p orbitals of chromium and from 2s and 2p orbitals of oxygen. A second distribution was generated by superposing the spherically averaged valence densities of the atoms constituting the molecule in a given electronic configuration (i.e., the promolecule), placed at the atomic positions in $[Cr(O_2)_4]^{3-}$, calculated by the Herman–Skillman method (the atomic Xα model),[56] with the same

(48) Coppens, P. *Angew. Chem., Int. Ed. Engl.* **1977**, *16*, 32.
(49) Coppens, P.; Stevens, E. D. *Adv. Quantum Chem.* **1977**, *10*, 1.
(50) Mrozek, J.; Smith, V. H.; Salahub, D. R.; Ros, P.; Rozendaal, A. *Mol. Phys.* **1980**, *41*, 509.
(51) McMaster, B. N.; Smith, V. H.; Salahub, D. R. *Mol. Phys.* **1982**, *46*, 449.
(52) Flack, H., to be submitted for publication.
(53) Benard, M.; Coppens, P.; DeLucia, M. L.; Stevens, E. D. *Inorg. Chem.* **1980**, *19*, 1924.
(54) Kutzler, F. W.; Swepston, P. N.; Berkovitch-Yellin, Z.; Ellis, D. E.; Ibers, J. A. *J. Am. Chem. Soc.* **1983**, *105*, 2996.
(55) Konowalow, D. D.; Weinberger, P.; Calais, J. L.; Connolly, J. W. D. *Chem. Phys. Lett.* **1972**, *16*, 81.

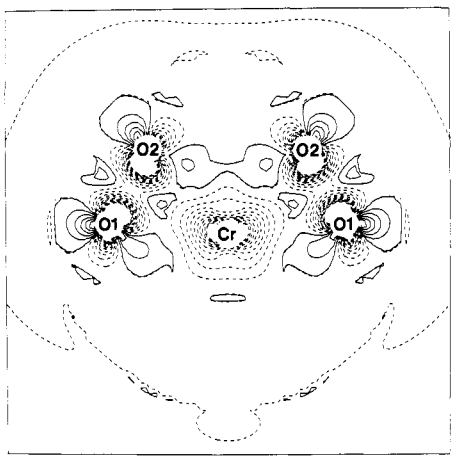

Figure 4. Valence deformation-density contours for $[Cr(O_2)_4]^{3-}$ in the 1, 1, 0 plane. Contour values differ by 0.10 e/Å^3; solid lines indicate positive contour values, dashed lines negative.

values of the atomic exchange parameter α as those used in the atomic spheres of the molecular calculation (Table I). In order to provide the deformation density, a point by point subtraction was then carried out for all of the 6561 points of the square mesh in the selected molecular plane. The choice of the electronic configuration of the atoms of the promolecule is delicate in our case, since there is no unique strategy for distributing the negative charge of the complex over the atoms. A good solution would be to perform a calculation for the K_3CrO_8 complex, i.e. introducing the first shell of potassium neighbors explicitly in the calculation. However, this solution had to be discarded because of the prohibitive amount of computer time it required. Instead, we decided to perform several calculations using different atomic configurations in the promolecule: starting from a standard configuration, obtained by assuming that the negative charge of 3- is equally distributed over the ligands (i.e., from the promolecule made of Cr^0 ($3d^6$) and $O^{0.375-}$ ($2s^2 2p_x^{1.4583} 2p_y^{1.4583} 2p_z^{1.4583}$), we used several test promolecules made of Cr^{n+} and $O^{(0.375-n/8)-}$ for $0 \leq n \leq 2$. Except for the region close to the metal atom, these calculations did not exhibit significant changes with respect to the case $n = 0$, and therefore we present here only the results obtained for this standard configuration.

The deformation densities calculated in a vertical plane bisecting the XOY angle (i.e., the 110 plane) are represented in Figure 4. This plane contains two MO_2 units (see Figure 1), and it is thus particularly interesting as it will reveal the displacement of so-called in-plane electrons (i.e., those lying in $\pi_g(\|)$, σ_g, and σ_u ligand orbitals and in d_{z^2}, d_{xy}, d_{xz}, and d_{yz} metal orbitals). The gross features of the contours in Figure 4 are readily understood when the populations of the p_σ, $p_{\pi(\|)}$, and $p_{\pi(\perp)}$ orbitals of oxygen are considered in the promolecule and in the molecule itself. In the spherically averaged $O^{0.375-}$ atom, the 4.375 p electrons are evenly distributed among p_σ, $p_{\pi(\|)}$, and $p_{\pi(\perp)}$ so that the occupation number of each is 1.4583. In the $[Cr(O_2)_4]^{3-}$ molecule, we have, according to Tables II, V, and VI, the following approximative configuration for oxygen: $p_\sigma^{0.96} p_{\pi(\|)}^{1.66} p_{\pi(\perp)}^{1.95}$. Thus, molecule formation from our promolecule involves an important transfer from p_σ to $p_{\pi(\|)}$ electrons, which shows up clearly in Figure 4. Indeed, one notices two important negative density peaks along the O–O bonds and correspondingly two positive accumulation zones around each oxygen atom at the approximative position of $\pi(\|)$ lobes. Furthermore, the presence of additional positive density peaks along these bonds in the π-bonding region reflects the importance of the contribution of π_u bonding MOs. In addition, it is interesting to notice the large zone of positive deformation density in the region located between the two O_2 atoms. This indicates that there is some long-range interaction between these atoms, which could also partly explain the structural distortion mentioned above, namely the large difference between $Cr-O_2$ and $Cr-O_1$ bond distances. Starting from a neutral metal atom in the promolecule, it is not surprising to find a large region of negative deformation density around this atom since we have previously shown (Table V) that the charge on chromium in the molecule is 1.42+. It is interesting to analyze in detail the shape of the contours in this region because it should reveal the dissymmetry in the distribution of 3d electrons around the metal atom. Indeed, using the metal configuration in the molecule presented in Table V and the spherical average over all the d components of the $3d^6$ configuration in atomic chromium (i.e., 1.2 electrons for each component), one is led to the following "configuration differences": $d_{z^2}^{-0.40}$, $d_{x^2-y^2}^{-0.14}$, $d_{xy}^{-0.60}$, $d_{xz}^{-0.48}$, $d_{yz}^{-0.48}$. In the (110) plane, the only deformation densities visible will be those due to d_{z^2} and d_{xy} and one notices clearly the two negative regions on the right and left sides of chromium due to the –0.60 population difference in d_{xy} and the swelling above this atom reflecting the –0.40 population difference in d_{z^2}. This rationalization accounts thus in a very reasonable way for the dissymmetry obtained in the deformation density of predominantly 3d electrons. Finally, let us mention that the above interpretation of the main features of the electron-deformation density in $[Cr(O_2)_4]^{3-}$ is coherent and consistent with previous conclusions drawn for other coordination compounds.[48,49,53,54] While this seems to indicate that the Xα model is adequate for such studies, a definite answer to this question will only be possible after extensive comparison with experimental results.

Hyperfine Interactions of ^{53}Cr in $[Cr(O_2)_4]^{3-}$. Dalal et al.[35] have recently reported variable-temperature EPR and magnetic susceptibility data measured for single crystals, powders, and solutions of K_3CrO_8, in order to obtain detailed information on the **g** tensor as well as the ^{53}Cr hyperfine tensor. Their results, which are complementary to previous EPR studies that did not employ single-crystal samples,[28,45] give considerable information on the ground-state electronic structure of the $[Cr(O_2)_4]^{3-}$ anion. They present both the absolute value and the sign of the unpaired density at the Cr nucleus, and they also establish that the unpaired electron is accommodated in a predominantly metal $d_{x^2-y^2}$ orbital exhibiting substantial delocalization over the dioxygen ligands.

We have shown recently[13,14] that the MS–Xα model is able to interpret and predict magnetic properties (such as the hyperfine interaction on metal) of paramagnetic coordination compounds reasonably well. It was thus interesting to broaden the scope of the present study by performing additional calculations of the ^{53}Cr hyperfine tensor parameters in order to provide a theoretical interpretation of the values deduced from EPR. It is well-known that, when the conventional spin Hamiltonian approach for interpreting EPR spectra is used,[57,58] the hyperfine tensor on the metal may be expressed in terms of several parameters, the most important ones being the zero-order isotropic Fermi contact contribution A_F and the first-order contribution to spin dipolar interaction, namely the anisotropic P parameter. We have shown previously[13,14] that the evaluation of A_F requires the use of the spin-polarized (SP, or spin-unrestricted) MS–Xα formalism

$$A_F = 8\pi/3 C_M[\rho^{\uparrow}(0) - \rho^{\downarrow}(0)]$$

(56) Herman, F.; Skillman, S. "Atomic Structure Calculations"; Prentice-Hall: Englewood Cliffs, NJ, 1963.

(57) Wertz, J. E.; Bolton, J. R. "Electron Spin Resonance"; McGraw-Hill: New York, 1972.

(58) Atherton, N. M. "Electron Spin Resonance"; Wiley: New York, 1973.

Table X. Contributions to the Fermi Contact Parameter of the ^{53}Cr Hyperfine Tensor of $[Cr(O_2)_4]^{3-}$ from SP-MS-Xα Calculations

orbital	energy, eV	n^a	$\rho(0)$,[b] au	$\rho\uparrow(0) - \rho\downarrow(0)$, au
$6a_1\uparrow$	−7.63	4	0.0039	−0.0003
$6a_1\downarrow$	−7.13	4	0.0042	
$5a_1\uparrow$	−10.29	4	1.6988	+0.0798
$5a_1\downarrow$	−10.30	4	1.6190	
$4a_1\uparrow$	−11.21	4	0.0336	+0.0077
$4a_1\downarrow$	−11.28	4	0.0259	
$3a_1\uparrow$	−19.70	4	0.0080	+0.0009
$3a_1\downarrow$	−19.80	4	0.0071	
$2a_1\uparrow$	−26.05	4	0.5292	+0.0117
$2a_1\downarrow$	−26.15	4	0.5175	
$1a_1\uparrow$	−76.14	3	53.1924	+0.2918
$1a_1\downarrow$	−74.26	3	52.9006	
Cr 2s↑	−662.06	2	374.2698	−0.5985
Cr 2s↓	−661.25	2	374.8683	
Cr 1s↑	−5833.79	1	4216.2210	−0.0180
Cr 1s↓	−5833.78	1	4216.2390	
				−0.2249 (total)

[a] Principal quantum number of the metal s component. [b] Electronic density at the Cr nucleus, defined as $\rho(0) = |u(0)|^2$, $u(r)$ being the corresponding wave function in metal sphere.

where $C_M = g_e\beta_e g_M\beta_M$, and $\rho^\uparrow(0)$ and $\rho^\downarrow(0)$ are the spin-up and spin-down electronic densities at the nucleus defined as

$$\rho^{\uparrow,\downarrow}(0) = \sum_s n_s^{\uparrow,\downarrow}|u_s^{\uparrow,\downarrow}(0)|^2$$

where the summation extends to all valence and core MOs, $u_s^{\uparrow,\downarrow}(r)$ having an s component in the metal sphere and $n_s^{\uparrow,\downarrow}$ being the occupation number of each MO.

On the other hand, the non-spin-polarized (NSP) formalism is generally sufficient for calculating the P parameter[13,14]

$$P = C_M\langle r^{-3}\rangle_{3d}$$

where $\langle r^{-3}\rangle_{3d}$ is the radial expectation value calculated over $R_{3d}(r)$, the metal 3d component of the open-shell MO in the NSP calculation. In order to correct for the error due to the truncation of the Xα wave function at the metal sphere, it is necessary to calculate $\langle r^{-3}\rangle_{3d}$ from an analytical multiple-ζ function of Slater type obtained by a fitting of the numerical $R_{3d}(r)$.[14]

Table X reports the individual contributions of the various orbitals with metal s components to the Fermi contact term A_F of the ^{53}Cr hyperfine tensor of $[Cr(O_2)_4]^{3-}$. It is seen that, in agreement with the conclusions of Dalal et al.,[35] the unpaired electron spin density at the chromium nucleus is negative, which implies that core-polarization effects, i.e. the polarization of the closed-shell electrons of the core by the open-shell orbital, are predominant. Indeed, inspection of the individual shell contributions shows that this negative resultant spin density is due to competition of different terms of opposite sign. However, while the 1s and 4s contributions to A_F are small, the major part of the Fermi contact coupling arises through 2s (negative) and 3s (positive) spin densities. This result is in agreement with both experiment[35] and the Hartree–Fock calculations of Watson and Freeman describing the origin of effective magnetic fields in transition metals;[59] lying inside the 3d, the 2s shell has its spin-up electrons attracted outward, leaving a region of negative spin density near the nucleus, and the effect is opposite for the 3s shell because of the close spatial proximity of 3s and 3d electrons. Using our calculated spin density of −0.2249 and the C_M value for chromium of -10.1×10^{-4} cm^{-1}/au derived from the data of Morton and Preston,[60] we find an A_F value of 19.0×10^{-4} cm^{-1} in very good agreement with the experimental result of 17.0×10^{-4} cm^{-1} (Table XI). This is a further confirmation of the good quality of the numerical Xα wave functions, whose full flexibility provides a quantitatively accurate description of the subtle mechanism of core polarization in coordination compounds.

Table XI. Comparison between Xα Results and Corresponding Values Deduced from EPR

property[a]	Xα[b]	exptl[c]	property[a]	Xα[b]	exptl[c]
A_F, 10^{-4} cm^{-1}	19.00	17.00	β^2	0.57	0.44
P, 10^{-4} cm^{-1}	−38.70	−25.00	γ^2	0.67	0.75
α^2	0.84	0.91			

[a] α^2, β^2, and γ^2 refer to the 3d charge distribution on metal of the $3b_1$, 9e, and $7b_2$ MOs, respectively. [b] This work. [c] Reference 35.

As to the P value, the NSP–Xα calculation performed using the radial part of the $3b_1$ MO gives $\langle r^{-3}\rangle_{3d} = 3.83$ au and consequently $P = -38.7 \times 10^{-4}$ cm^{-1}. The agreement with experiment is here less satisfactory (Table XI) since Dalal et al. report the result -25.0×10^{-4} cm^{-1}. However, this value has not been obtained directly from the experiment but deduced as a solution of a system of self-consistent equations yielding simultaneously A_F and the parameters α^2, β^2 and γ^2, which denote the metal 3d charge distributions of the $3b_1$, 9e, and $7b_2$ MOs, respectively. Taking into account that the value of $\langle r^{-3}\rangle_{3d}$ increases as a function of the positive charge on the metal (because of the corresponding contraction of the 3d shell) and that Morton and Preston[60] report a P value of -34.5×10^{-4} cm^{-1} for neutral chromium, the result of Dalal et al. seems questionable, leading to a value smaller (in absolute value) than the result for neutral chromium. On this basis, we therefore suggest that the value of the P parameter of ^{59}Cr hyperfine tensor should be of the same order or slightly larger in absolute value than this atomic result, and this would lead to a better agreement with the Xα result. Finally, we compare also in Table XI the calculated vs. the experimental values of the α^2, β^2, and γ^2 parameters. It is seen that both sets of values are in reasonable overall agreement. It is particularly gratifying to remark on the good accord concerning the covalency of the $3b_1$ open-shell MO. In summary, the present calculations allow description in a very reasonable way the hyperfine interactions on the metal in $[Cr(O_2)_4]^{3-}$, which suggest that the MS–Xα model can actually be used as a sound descriptive and predictive model for the interpretation of EPR data obtained for coordination compounds.

Acknowledgment. This work is part of Projects 2.132-0.78 and 2.615-0.82 of the Swiss National Science Foundation. The Computer Center of the University of Geneva is gratefully acknowledged for a grant of computer time.

Registry No. $[Cr(O_2)_4]^{3-}$, 12526-97-5; $[Mo(O_2)_4]^{2-}$, 42489-15-6; $[Nb(O_2)_4]^{3-}$, 51456-19-0.

(59) Watson, R. E.; Freeman, A. J. *Phys. Rev.* **1961**, *123*, 2027.

(60) Morton, J. R.; Preston, K. F. *J. Magn. Reson.* **1978**, *30*, 577.